Dimerization and Folding Processes of *Treponema denticola* Cystalysin: The Role of Pyridoxal 5′-Phosphate†

Barbara Cellini,‡ Mariarita Bertoldi,‡ Riccardo Montioli,‡ Douglas V. Laurents,§ Alessandro Paiardini,|| and Carla Borri Voltattorni*,‡

Dipartimento di Scienze Morfologico-Biomediche, Sezione di Chimica Biologica, Facoltà di Medicina e Chirurgia, Università degli Studi di Verona, Strada Le Grazie, 8, 37134 Verona, Italy, Instituto de Quimica-Fisica "Rocasolano", Consejo Superior de Investigaciones Cientificas, Serrano 119, E-28006 Madrid, Spain, and Dipartimento di Scienze Biochimiche "A. Rossi Fanelli" and Centro di Biologia Molecolare del Consiglio Nazionale delle Ricerche, Università "La Sapienza", 00185 Roma, Italy

Received July 25, 2006; Revised Manuscript Received October 4, 2006

ABSTRACT: Cystalysin, the key virulence factor in the bacterium *Treponema denticola* responsible for periodontitis, is a homodimeric pyridoxal 5′-phosphate (PLP)-C-S lyase. The dimerization process and the urea-induced unfolding equilibrium of holocystalysin were compared with those of the apo form. The presence of PLP decreases ∼4 times the monomer−dimer equilibrium dissociation constant. By using a variety of spectroscopic and analytical procedures, we demonstrated a difference in their unfolding profiles. Upon the monomerization of apocystalysin, occurring between 1 and 2 M urea, a self-associated equilibrium intermediate with a very high β-sheet content is stabilized over the 2.5−4 M urea range, giving rise to a fully unfolded monomer at higher urea concentrations. On the other hand, highly destabilizing conditions, accompanied by the formation of a significant amount of insoluble aggregates, are required for PLP release and monomerization. Refolding studies, together with analysis of the dissociation/association process of cystalysin, shed light on how the protein concentration and the presence or absence of PLP under refolding conditions could affect the recovery of the active dimeric enzyme and the production of insoluble aggregates. When the protein is completely denatured, the best reactivation yield found was ∼50% and 25% for holo and apocystalysin, respectively. The dimerization and folding processes of cystalysin have been compared with those of another PLP C-S lyase, MalY from *E. coli*, and the possible relevance of their PLP binding mode in these processes has been discussed.

Cystalysin (E.C.4.4.1.1) was identified as a virulence factor of the human oral pathogen *Treponema denticola* and is endowed with hemeolytic and hemeoxidative activities leading to both tooth and gum damage (*1*). Successive studies demonstrated that cystalysin is a homodimeric, pyridoxal 5′-phosphate (PLP[1])-dependent enzyme, which catalyzes the α,β-elimination of L-cysteine to produce pyruvate, ammonia, and H_2S (*2*). Interestingly, cystalysin toxicity has been directly related to the production of H_2S, a compound that is toxic to most cells at high concentrations (*2*). The enzyme has a broad substrate specificity and accepts several sulfur- and non-sulfur-containing amino acids as well as disulfidic amino acids as substrates (*3*). Additionally, cystalysin catalyzes as side reactions the racemization and overall transamination of both enantiomers of alanine (*4*).

The atomic resolution structure of cystalysin has been reported (*5*). The overall structure of the enzyme is similar to that observed for the proteins belonging to the fold-type I family of PLP-enzymes. The cystalysin monomer consists of two domains: the large domain (residues 48−288), carrying the PLP cofactor covalently bound to Lys238, whose central element is a mainly parallel seven-stranded β-sheet that is found in all members of the aminotransferases family, and the small domain formed by the N (residues 1−47)- and C (288−394)-terminal of the polypeptide chain. Both domains form a deep cleft in the center of the cystalysin monomer, at the bottom of which PLP is bound to the C-terminal end of the seven-stranded β-sheet (Figure 1).

In recent years, most of the work on cystalysin, performed by means of kinetic and site-directed mutagenesis studies, was focused on the elucidation of the substrate and reaction specificity (*3*) and on the identification of catalytic residues (*6*−*8*). Thus, on the basis of crystal structure and these investigations, evidence has been provided on some mechanistic aspects of the reactions catalyzed by cystalysin (*6*−*8*). There is, however, no report to date on the folding mechanism of cystalysin.

In this work, we employ a variety of biophysical techniques and analytical procedures to characterize the dimerization process and the urea-induced folding equilibrium of

† This work was supported by funding from the Italian Ministero dell'Università e Ricerca Scientifica e Tecnologica (to C.B.V.).

* Corresponding author. Tel: +39-045-8027-175. Fax: +39-045-8027-170. E-mail: carla.borrivoltattorni@univr.it.

‡ Università degli Studi di Verona.

§ Consejo Superior de Investigaciones Cientificas.

|| Università "La Sapienza".

[1] Abbreviations: PLP, pyridoxal 5′-phosphate; DLS, dynamic light scattering; ANS, 8-anilino-1-naphtalenesulphonic acid; *R*s, Stokes radius.

10.1021/bi061496l CCC: $33.50
Published on Web 11/07/2006

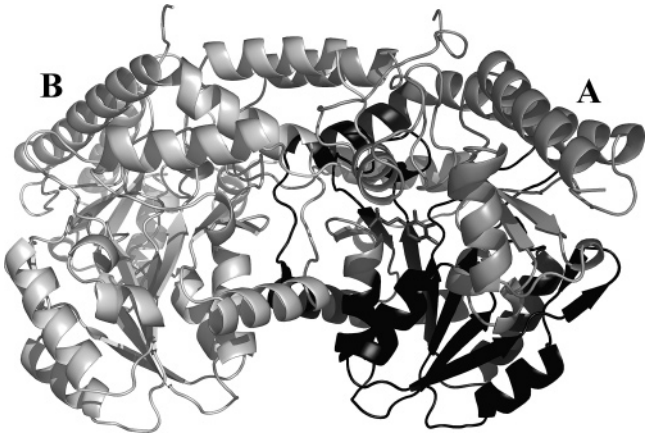

FIGURE 1: Schematic representation of the structure of *T .denticola* holocystalysin. Ribbon representation of the dimeric form of cystalysin (pdb code: 1c7n), showing the domain organization of the enzyme. The major and minor domain of chain A are depicted as dark and light gray ribbons, respectively. Chain B is colored in white. The PLP moiety of chain A is also represented, as black sticks.

cystalysin. Our results, in addition to indicating that cystalysin's stability is augmented by the presence of the coenzyme, provide some insight into the effect of PLP on the association equilibrium between monomer and dimer and the folding process of this PLP enzyme. Furthermore, the association/dissociation process and the urea-induced folding pathway of cystalysin have been compared with those recently reported for *E. coli* MalY (*9*), a PLP-dependent Cβ-Sγ lyase member of the type I fold family of PLP enzymes. Cystalysin and MalY have a very low degree of sequence similarity but bear a significant structural resemblance.

EXPERIMENTAL PROCEDURES

Materials. PLP, urea, β-chloro-L-alanine, NADH, lactate dehydrogenase, dithiothreitol, and glutaraldehyde were obtained from Sigma. 8-Anilino-1-naphtalenesulphonic acid (ANS) was purchased from Molecular Probes. All other chemical probes were of the highest purity available.

Expression and Purification of Cystalysin. Cloning, expression, and purification of cystalysin were carried out as described earlier (*3*). Apocystalysin was prepared as previously described (*3*). The enzyme concentration was determined using the molar absorption coefficient $\epsilon_M = 1.27 \times 10^5$ M^{-1} cm^{-1} at 281 nm (*3*). The PLP content of holocystalysin was determined by releasing the coenzyme in 0.1 M NaOH and by using $\epsilon_M = 6600$ M^{-1} cm^{-1}at 388 nm (*10*).

Urea Denaturation. Cystalysin in the holo or apo form (1 μM) was dissolved in potassium phosphate buffer (20 mM, pH 7.4) in the absence or presence of increasing concentrations of urea and incubated for 15 h at 25 °C before the measurements were made. The actual urea concentration was checked using refractive index data (*11*). The unfolding equilibrium of holo and apocystalysin was determined by following the changes in structural and functional signals as detailed below. To establish the time required to reach equilibrium, the enzyme properties at any urea concentration were measured as a function of time until no further changes were observed.

Enzymatic Activity. During the purification of cystalysin, enzymatic activity was determined by measuring pyruvate formation from β-chloro-L-alanine by a spectrophotometric assay coupled with the NADH-dependent lactate dehydrogenase (*3*). In the experiments designed to determine the effect of various concentrations of urea on lyase activity of cystalysin, pyruvate production from β-chloro-L-alanine was measured by an assay based on measuring the dinitrophenylhydrazine derivative of pyruvate, as reported previously (*12*, *13*).

Fluorescence Spectroscopy. All fluorescence measurements were performed by using a 1-mL cell in a Jasco FP-750 instrument equipped with a thermostated cell holder. Tryptophan emission spectra were taken from 300 to 550 nm using an excitation wavelength of 281 nm, and 5 nm excitation and emission bandwidths. Steady-state fluorescence measurements were performed at 25 °C at 1 μM protein concentration. Each spectrum was corrected by subtracting the emission of the buffer at the same urea concentration. For ANS binding experiments, cystalysin at 1 μM concentration was first equilibrated at the desired urea concentration overnight at 25 °C. Then a stock solution of ANS was added to a final concentration of 15 μM and incubated at 25 °C for 1 h. The excitation wavelength was 365 nm, and the emission was recorded from 400 to 560 nm. The values were normalized by subtracting the baseline recorded for the probe alone under identical conditions. To determine the emission maximum position, fluorescence spectra were processed by Jasco software.

CD Measurements. CD spectra were recorded on a Jasco J-710 spectropolarimeter equipped with a constant temperature cell holder. Conformational changes in the secondary structure of cystalysin were monitored in the region between 210 and 260 nm, and the path length was 0.1 cm, while changes in the tertiary structure were observed in a cuvette with a path length of 1 cm in the near-UV region (260−320 nm). The release of PLP from holocystalysin was monitored by the decrease in the CD signal at 418 nm with increasing urea concentrations. Protein concentration in all CD measurements was 1 μM. For each sample, three spectra were recorded at a scan speed of 50 nm/min with a bandwidth of 2 nm and averaged automatically. Spectra were corrected by subtracting the contribution of the solvent with the same denaturant concentration. The secondary structure content of cystalysin was determined by the neural net deconvolution procedure of Böhm et al. (*14*) using a set of 33 proteins.

Size-Exclusion Chromatography. The oligomeric state and the hydrodynamic dimensions of holo and apocystalysin, in the absence or presence of varying urea concentrations, were determined by comparing elution volumes to a set of molecular weight standards of known Stokes radius (*R*s) on a Superdex 200 10/300 GL column equilibrated and run with a potassium phosphate buffer (20 mM, pH 7.4) containing the desired urea concentration. An ÄKTA FPLC system (GE Healthcare) was used. A volume of 200 μL of the standard mixture or 1 μM cystalysin solution, after incubation at the desired urea concentration for 15 h at 25 °C, was loaded onto the column and run at 25 °C with a flow rate of 0.2 mL/min and detection at 280 nm. Each sample was injected in triplicate, and the elution volume (V_e) was identified using the software Unicorn 5.01 (Amersham Biosciences). According to the method of Uversky (*15*), a calibration curve was generated by measuring the V_e and plotting the migration rate ($1000/V_e$) versus *R*s for each protein standard in native

forms at 0 M urea and in their unfolded forms at 8 M urea. The data on the entire set fit to the following expression

$$1000/V_e = (0.732 \pm 0.022)Rs + (43.6 \pm 1.1)$$

from which the experimental *R*s values of holo and apocystalysin in their native, partially unfolded and unfolded states were determined.

The monomer−dimer dissociation constant of cystalysin was estimated using the method of Manning et al. (*16*). Briefly, a stock solution of cystalysin was dissolved in 20 mM potassium phosphate buffer at pH 7.4 to different protein concentrations. Each mixture was incubated at 25 °C for 2 h (a sufficient time to reach the equilibrium between monomer and dimer) and then loaded onto a Superdex 200 10/30 GL column equilibrated with the same buffer. Elution volumes have been analyzed in terms of the average peak concentration, which is calculated as (sample volume) × (sample concentration)/(peak volume), where the total peak volume is estimated to be equivalent to the volume at half-peak height.

Dynamic Light-Scattering (DLS) Measurements. Samples were prepared at a final cystalysin concentration of 1 μM in a potassium phosphate buffer at pH 7.4 in the absence or presence of various concentrations of urea. Each protein sample was prepared by diluting a stock solution, and after incubation for 15 h at 25 °C, a 500 μL-volume disposable cuvette (12.5 mm × 12.5 mm × 45 mm) with 1 cm light path was used. Data were obtained with a Zetasizer Nano S DLS instrument (Malvern Instruments Ltd., Worcestershire, U.K.), setting the appropriate viscosity and refractive index parameters for each solution and keeping the temperature at 25 °C during the measurements by means of a Peltier thermostating system. The buffer was filtered immediately before use to eliminate any impurities.

Cross-Linking Experiments Using Glutaraldehyde. Cystalysin (1 μM) was incubated at the desired concentration of urea for 15 h at 25 °C. Glutaraldehyde was added to a final concentration of 1%. The samples are incubated at 25 °C for 5 min followed by quenching the cross-linking reaction by the addition of 200 mM sodium borohydride. After 20 min of incubation, 3 μL of aq. 10% (v/v) sodium deoxycholate was added. The protein was precipitated by the addition of orthophosphoric acid so as to bring the pH to 2−2.5. The sample was centrifuged, and the pellet was suspended in sample buffer for analysis on SDS−PAGE (7.5% polyacrylamide). The cross-linking reaction in native conditions resulted in a cross-linked dimer in addition to a detectable amount of uncross-linked monomer and minimal traces of higher order cross-linked products. Bands were visualized after staining with Coomassie Blue, and their intensities were analyzed using ImageJ quantitation software (Wayne Rasband, NIH, Bethesda, MD).

NMR Spectroscopy. One-dimensional ^{1}H NMR spectra of holocystalysin dissolved in 0, 4, and 8 M urea and apocystalysin dissolved in 0 and 8 M urea were recorded on a Bruker 600 MHz AMX spectrometer equipped with a cryoprobe for increased sensitivity. Although the urea and buffer solutions were prepared in D_2O to reduce the H_2O solvent resonance, the D/H ratio in the final sample was about 5:1 because of the presence of H_2O in the cystalysin stock solution. The presence of some H_2O is advantageous because it permits the observation and characterization of the amide and indole resonances under denaturing conditions. Samples contained 50 μM sodium 4,4-dimethyl-4-silapentane-1-sulfonate as the internal chemical shift reference and were buffered by 20 mM potassium phosphate at pH* 7.4 (where pH* stands for the pH meter reading in D_2O uncorrected for the deuterium isotope effect). Deuterated urea was prepared by repeated exchange/lyophilization of urea in D_2O. The concentration of urea stock solutions was determined by refractive index (*11*).

In one experiment, three samples containing 0, 4, and 8 M urea were incubated at 25 °C overnight (15−18 h) before recording their NMR spectra (400 transients per spectrum). In a second experiment, a series of 18 spectra (one spectrum per hour; 256 transients per spectrum) were recorded on a sample of holocystalysin dissolved in 8 M urea. The final cystalysin concentration was 108 μM in the first experiment and 175 μM in the second experiment. All spectra were recorded at 25.0 °C. Presaturation was used to suppress the residual H_2O signal. The data were Fourier-transformed and analyzed using the supplied Bruker software.

Refolding of Cystalysin. For the kinetic determination of the renaturation, holocystalysin was first denatured in 8 M urea in 20 mM potassium phosphate buffer at pH 7.4 at 25 °C for 15 h. The denatured enzyme was 100-fold diluted into the same buffer without the denaturant containing 0.5 mM dithiothreitol. At various times, aliquots were removed for enzyme activity assays. To follow reactivation after treatment at different concentrations of urea, the protein (1 or 5 μM) was incubated at the indicated concentration of denaturant for 15 h at 25 °C, and then it was diluted 100-fold into the buffer without urea. Alternatively, refolding was performed by extensive dialysis of the urea-treated holo or apocystalysin against 20 mM potassium phosphate buffer at pH 7.4, containing 0.5 mM dithiothreitol, with or without 100 μM PLP.

Calculation of Accessible Surface Areas. The accessible surface area (ASA) buried upon dimerization was calculated with the program NACCESS (*17*), which makes use of the algorithm by Lee and Richards (*18*), whereby a probe of given radius is rolled around the surface of the molecule, and the path traced out by its center is the accessible surface. The crystal structure of cystalysin from *Treponema denticola* (pdb code: 1C7N) (*5*) with a probe radius of 1.4 Å and a slice width of 0.1 Å was used for the calculation. To estimate the variation in solvent accessible surface area (ΔASA) during complex formation, the total polar and nonpolar surface areas of the monomeric and dimeric states were calculated. The identity of the residues forming the interface and the change in total polar or nonpolar accessible surface areas was then determined by subtracting the ΔASA in the dimeric state from that for the monomeric state for each residue. A residue was considered to form part of the interface when its ΔASA was >1 Å^2 (*19*). Hydrogen bonds were calculated using the program HBPLUS (*20*). Salt bridges have been calculated using the 4.0 Å cutoff (*21*). The volume of the gaps between interacting subunits was calculated using a program SURFNET (*22*).

Phase Diagram Method. The use of phase diagrams to detect folding intermediates was generalized by Kuznetsova et al. (*23*) to any extensive parameter. The essence of this approach, applied to our fluorescence data, is to plot a

diagram of $I_{\lambda 1}$ versus $I_{\lambda 2}$, where $I_{\lambda 1}$ and $I_{\lambda 2}$ are the fluorescence intensity values measured at wavelengths $\lambda 1$ and $\lambda 2$, respectively, under the different experimental conditions for a protein undergoing structural transformations. With regard to protein unfolding, it is possible to derive a relationship between $I_{\lambda 1}$ and $I_{\lambda 2}$, predicting that the dependence $I_{\lambda 1} = f(I_{\lambda 2})$ will be linear if changes in protein environment lead to the all-or-none transition between two different conformations.

Data Analysis. The analysis of the equilibrium unfolding curves corresponding to a two-state model (N ⇔ U) was performed according to eq 1

$$Y = \frac{Y_N + Y_U e^{-m(C_m - C)/RT}}{1 + e^{-m(C_m - C)/RT}} \quad (1)$$

where Y is the observed variable parameter, Y_N and Y_U are the values characteristic of the native (N) and fully unfolded (U) conformations, respectively, C denotes the urea concentration, C_m is the midpoint of urea required for unfolding, and m stands for the slope of the unfolding curve at C_m.

The urea-unfolding curves corresponding to a three-state denaturation pathway (N ⇔ I ⇔ U, where I is the intermediate state) or a four-state denaturation pathway (N ⇔ I_1 ⇔ I_2 ⇔ U) were analyzed using eq 2 or 3, respectively:

$$Y = \frac{Y_{N-I_1}[\text{urea}]^{n1}}{C_{m1}^{n1} + [\text{urea}]^{n1}} + \frac{Y_{I-U}[\text{urea}]^{n2}}{C_{m2}^{n2} + [\text{urea}]^{n2}} \quad (2)$$

$$Y = \frac{Y_{N-I_1}[\text{urea}]^{n1}}{C_{m1}^{n1} + [\text{urea}]^{n1}} + \frac{Y_{I_1-I_2}[\text{urea}]^{n2}}{C_{m2}^{n2} + [\text{urea}]^{n2}} + \frac{Y_{I_2-U}[\text{urea}]^{n3}}{C_{m3}^{n3} + [\text{urea}]^{n3}} \quad (3)$$

in which C_{m1}, C_{m2}, and C_{m3} are the midpoint concentrations of urea, $Y_{N\leftrightarrow I}$ (or $Y_{N\leftrightarrow I1}$), $Y_{I1\leftrightarrow I2}$, and $Y_{I\leftrightarrow U}$ (or $Y_{I2\leftrightarrow U}$) represent the change in the signal for the N ⇔ I (or N ⇔ I_1), I_1 ⇔ I_2, and I ⇔ U (or I_2 ⇔ U) transitions, respectively, and exponents n_1, n_2, and n_3 reflect the steepness of the transition between states as a function of urea concentration.

The subunit dissociation constant (K_d) in apocystalysin in the absence or presence of PLP was determined according to (*16*) the following equation:

$$\%D = [(8[E] + K_d) - (K_d^2 + 16K_d[E])^{1/2}]/0.08[E] \quad (4)$$

where $\%D$ is the percentage of dimer or maximal specific activity to total enzyme, and [E] represents the total concentration of enzyme in dimer equivalents. A plot of log[$(\%D/0.04(100 - \%D)^2)$] with respect to log[E] yields a straight line of slope 1. When $[(\%D/0.04(100 - \%D)^2)] = 1$, $K_d = [E]$.

RESULTS

Equilibrium Unfolding Studies of Cystalysin: Spectroscopic, Enzymatic Activity and Molecular Dimensions Experiments. Different conformational states during the urea-induced unfolding of cystalysin in the holo and apo forms have been identified using a multiparametric approach, which involves the application of several physicochemical methods (absorbance, fluorescence, circular dichroism, ANS fluorescence, NMR, DLS, size-exclusion chromatography, and cross-linking) sensitive to the various structural levels of the protein. All experiments were performed at 1 μM protein concentration except for NMR analysis, which requires a higher protein concentration.

Holocystalysin. As previously reported (*3*), holocystalysin exhibits an emission spectrum (exc. at 281 nm) centered at 336 nm and a near-UV CD spectrum characterized by a negative dichroic band at 288−296 nm. Far-UV CD spectra of native holocystalysin indicate a composition of secondary structure elements that is in good agreement with that evaluated from crystallographic data. In the presence of increasing concentrations of urea, a red shift of the fluorescence emission band and a decrease of the 288 nm CD signal (Figure 2A) (both reporting the microenvironment of the side chain aromatic rings) as well as a progressive loss of the far-UV CD signal at 222 nm (Figure 2B) (which reflects a loss of helical structure) were observed. Typical unfolding profiles for holocystalysin as monitored by emission maximum fluorescence (exc. at 281 nm), near-, and far-UV CD are shown in Figure 2C. It should be noted that the emission intensity of the holoenzyme remains almost invariant over the entire range of urea concentrations examined. This behavior was likely due to a cancellation of two opposing effects: the decreased energy transfer from tryptophan to PLP (which increases tryptophan's emission) and the increased quenching of tryptophan by the solvent as this aromatic residue becomes more exposed (this effect decreases emission). Although the curves reported in Figure 2C are not exactly coincidental, all three of them describe a two-state process with a midpoint of transition of ∼4 M urea (Table 1). The urea-induced unfolding of the enzyme was also monitored by visible CD and enzymatic activity experiments. The internal aldimine of cystalysin exhibited an absorption band centered at 418 nm, associated with a positive dichroic signal (*3*). The loss of the CD signal at 418 nm was observed with increasing urea concentrations, and as reported in the inset of Figure 2C, the data are fit to a two-state model (eq 1). The midpoint of the transition, C_m, occurs at ∼3.1 M urea (Table 1). Lyase activity of holocystalysin was lost via a single transition with a $C_m = 3.04 \pm 0.06$ M urea (inset of Figure 2C and Table 1), coincident with that observed by visible CD, thus suggesting that the loss of PLP from the enzyme results in the loss of enzymatic activity. Because the noncoincidence of the various unfolding curves is considered as an argument in a favor of the intermediate state accumulation, we decided to use the method of phase diagrams (*23*), which is a powerful tool for uncovering hidden intermediates. Figure 3A, representing a parametric diagram of fluorescence intensity at 320 nm (I_{320}) versus fluorescence intensity at 365 nm (I_{365}), provides evidence that holocystalysin unfolding is a complex process. One can see that urea-induced unfolding of holocystalysin consists of at least three linear segments: 0−2, 2−5, and 5−10 M urea. This reflects the existence of at least three independent transitions separating four conformational states.

After detecting the existence of equilibrium intermediates, we next consider experimentation aimed to assess the effect of urea on the molecular dimensions of the holoenzyme by DLS, size-exclusion chromatography, and cross-linking studies. These experiments were performed on holocystalysin samples (1 μM) in the absence or presence of various concentrations of urea. The peak at 8.4 ± 0.3 nm observed

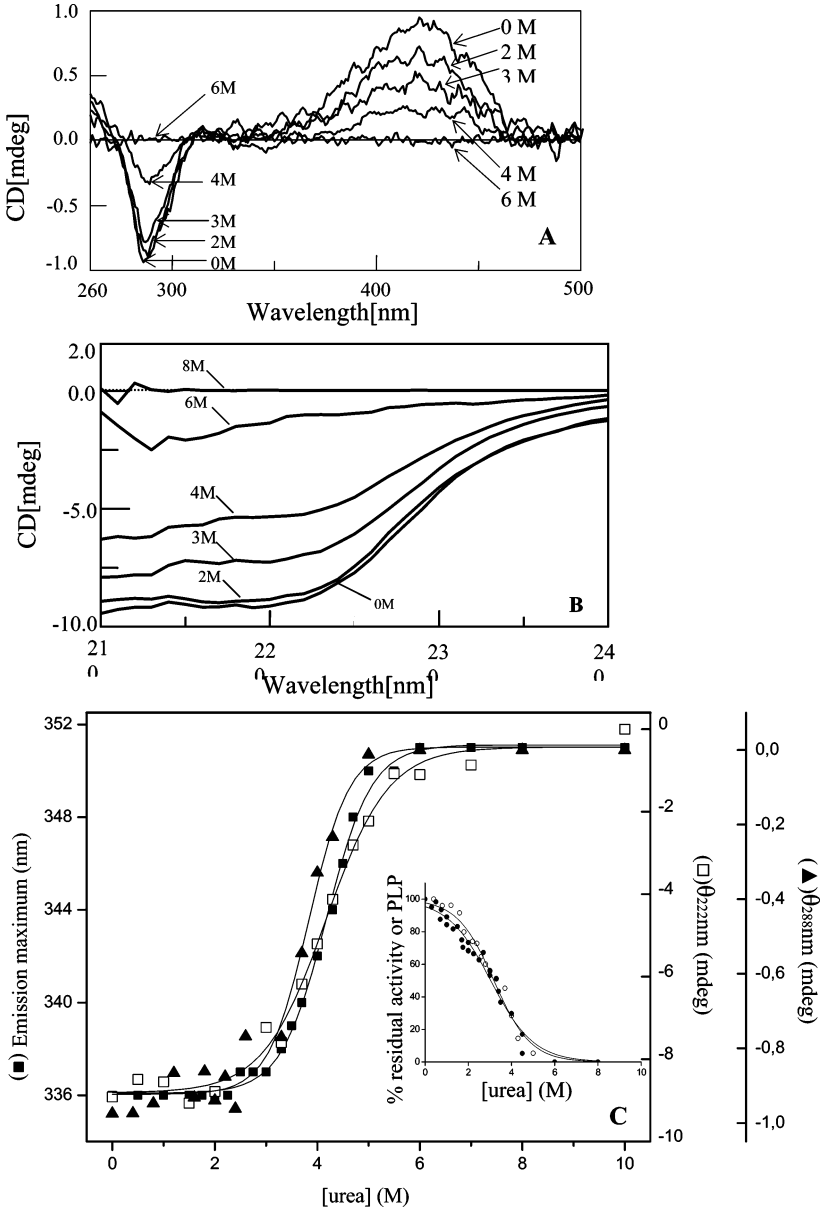

FIGURE 2: Urea-induced unfolding equilibrium of holocystalysin. (A) Near-UV, visible, and (B) far-UV CD spectra of holocystalysin in the absence and presence of urea at the indicated concentrations. (C) Unfolding profiles of holocystalysin monitored by emission maximum fluorescence (excitation at 281 nm) (■), far-UV CD at 222 nm (□), and near-UV CD at 288 nm (▲). (Inset) Changes in enzymatic activity (●) and in visible CD spectroscopy measured at 418 nm (○) for holocystalysin. The solid lines represent the best fit obtained using a two-state denaturation model (eq 1). The data shown are the means of four independent experiments; The S.E. of the mean (not shown) was less that 5% of the mean value in every case. In all of the unfolding experiments, the protein concentration was 1 μM, and the buffer was 20 mM potassium phosphate at pH 7.4.

without the denaturant (Figure 4A) is consistent with the hydrodynamic diameter of holocystalysin determined by X-ray crystallography (*5*). As shown in Figure 4B, the native dimer of holocystalysin elutes as a single peak from a size-exclusion column with a retention volume of 14.3 mL corresponding to an experimental *R*s of 3.6 nm. Between 0 and 5 M urea, the enzyme displays an increased hydrodynamic diameter (up to 12.2 ± 0.7 nm) and elutes with a decreased retention volume (up to 13.5 mL, corresponding to an experimental *R*s of 4.2 nm). It is worth pointing out that these species still bind PLP, as demonstrated by HPLC analysis of the supernatant obtained by deproteinization of the collected peaks. Additionally, the progressive generation of insoluble aggregates could be observed either by the appearance in DLS experiments of enzymatic species with a hydrodynamic diameter ranging from 140 to 200 nm or by a significant decrease in the size-exclusion column of the total peak area of the unfolded protein. Finally, from 5 to 8 M urea, the population of insoluble aggregates was gradually converted into the soluble unfolded monomer characterized by a retention volume of 11.4 mL (corresponding to an experimental *R*s of 12 nm) and by a peak area approximately 80% and 100% with respect to that of native holo and apocystalysin, respectively (see below in the apocystalysin section). DLS measurements of enzyme at 6 M urea reveal an ensemble of species with a hydrodynamic diameter of 72 ± 18 nm, which can be attributed to a mixture of aggregates and an incompletely unfolded monomer. It should be noted that on the basis of an empirical equation to measure hydrodynamic radii of native and denatured proteins (*24*), the calculated hydrodynamic diameter of the native dimer and fully denatured monomer of cystalysin was found to be

Table 1: C_m Values for Urea-Induced Unfolding Holo and Apocystalysin Monitored by Various Signals at an Enzyme Concentration of 1 μM[a]

probe	holoenzyme (M)	apoenzyme (M)
enzymatic activity	3.04 ± 0.06	1.1 ± 0.1 2.10 ± 0.02
CD visible	3.19 ± 0.06	
tryptophan fluorescence		
emission maximum	4.2 ± 0.3	2.25 ± 0.02 3.95 ± 0.04
relative intensity		1.1 ± 0.1 2.20 ± 0.02 4.1 ± 0.1
near UV CD	3.8 ± 0.1	2.10 ± 0.02
far UV CD	4.2 ± 0.4	3.95 ± 0.04

[a] A single value of C_m resulted from fitting data to a two-state process (eq 1), two C_m values and three C_m values resulted from fitting data to a three-state process (eq 2) or a four-state process (eq 3), respectively.

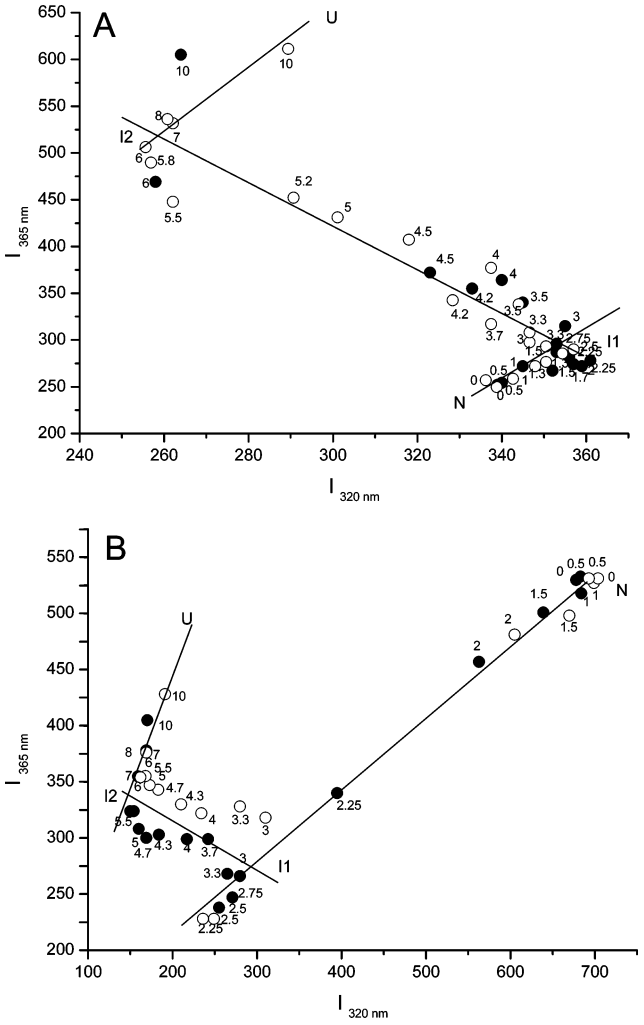

FIGURE 3: Phase diagram representing urea-induced unfolding of (A) holo and (B) apocystalysin. Filled and open symbols correspond to two independent sets of experiments. Each straight line represents an all-or-none transition between two conformers. N, I_1, I_2, and U represent native, intermediate 1, intermediate 2, and unfolded species, respectively. The denaturant concentration values are indicated in the vicinity of the corresponding symbol.

10.8 ± 3.3 and 13.4 ± 6.8 nm, respectively. Taken together, these data indicate a good agreement between experimental *R*s measured either by DLS or size-exclusion chromatography, except in urea concentration range where aggregates appear. Glutaraldehyde cross-linking experiments at different urea concentrations were performed to follow the denaturation profile of holocystalysin. At low denaturant concentrations (0−3 M urea), there is no significant decrease in the relative population of dimer to monomer, indicating the absence of a monomeric intermediate. Moreover, from 3 to 5 M urea, very large aggregates appear. At high denaturant concentration after complete unfolding (8 M urea), only monomers were detected (Figure 4C). The midpoint of dimer dissociation is 3.9 ± 0.1 M; this is consistent with the midpoints for dimer unfolding obtained by fluorescence spectroscopy and circular dichroism. Although the results are somewhat noisy, given the nature of the method, it is clear that dissociation does not precede unfolding.

In an attempt to establish whether hydrophobic interactions are involved in the formation of aggregated species, the effect of urea-induced changes in holocystalysin on the exposure of buried hydrophobic clusters was studied by using the hydrophobic fluorescent probe ANS. The binding of this probe to solvent-accessible clusters of nonpolar side chains in proteins results in a marked increase in fluorescence accompanied by a blue-shift in its emission fluorescence spectrum. Upon the addition of native holocystalysin to ANS, the fluorescence is characterized by an emission maximum at 497 nm and a slight increase of emission intensity. No significant changes of the ANS emission intensity over the 0−10 M urea range have been observed. However, a shift of the emission maximum begins at 4 M urea, reaching the same value at 6 M as if holocystalysin were not present (data not shown). These data suggest that no hydrophobic patches become exposed during urea-induced unfolding of holocystalysin.

NMR spectroscopy was also used to monitor the unfolding pathway of holocystalysin. The 1D ^{1}H NMR spectrum of cystalysin in 0 M urea after overnight incubation at 25 °C shows broad resonances typical of a large folded protein (Figure 5A). Several signals appear in the upfield region (0.1 to −1.5 ppm) of the spectrum (Figure 5A, inset). Such signals typically arise from methyl and methylene protons stacked on aromatic groups in the folded protein core (*25*). The broad signals appearing from 8 to 10.5 ppm are due to amide and indole protons.

After overnight incubation at 25 °C, the sample of cystalysin dissolved in 4 M urea appeared somewhat cloudy. After centrifuging the sample, a white deposit appeared in the bottom of the tube, and the protein solution was a clear yellow color. The whiteness of the deposit suggests that it is formed by aggregates of apocystalysin (see below). The solution remained clear during and after the recording of the NMR spectrum. The NMR spectrum of the sample in 4 M urea is similar to that in 0 M urea in the αH and βH regions (4.5 to 2.0 ppm) (Figure 5B). More differences are seen below 1 ppm; although the upfield signals persist, they are weaker and broader, and the signal at 0.9 ppm assignable to unfolded $-CH_2-$ and $-CH_3$ groups shows a slightly increased intensity relative to the spectrum recorded in 0 M urea. Additional changes are observed in the aromatic region of the spectrum (6.5 to 8.0 ppm).

The spectrum recorded 30 min after dissolving the protein in 8 M urea reveals sharp resonances associated with a

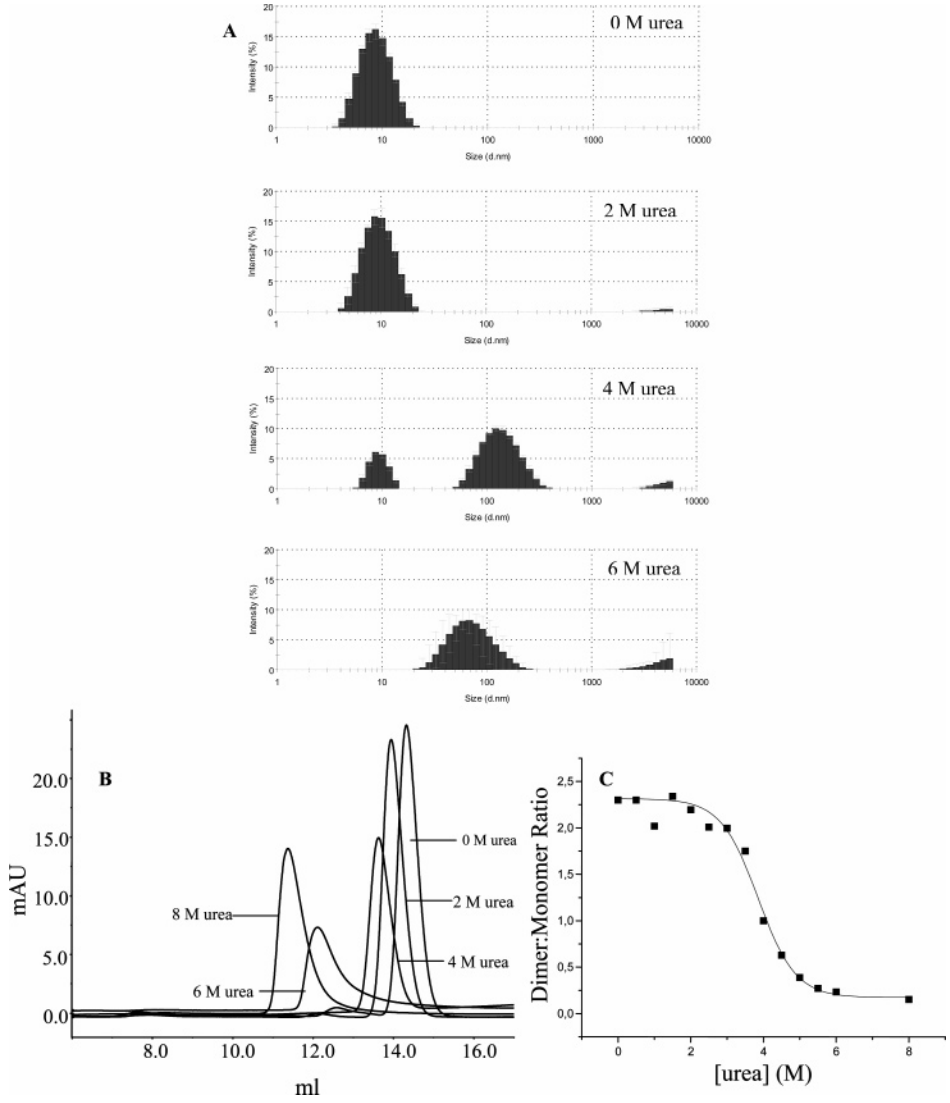

FIGURE 4: Urea-induced changes in molecular dimension of holocystalysin. (A) Size distribution from DLS and (B) chromatographic profiles on the Superdex 200 HR/30 column of holocystalysin at the indicated urea concentrations. (C) Glutaraldehyde cross-linking of holocystalysin. Ratios of band intensities obtained from SDS−PAGE corresponding to the chemically cross-linked dimer relative to the monomer are plotted at increasing urea concentrations. Both monomer and dimer bands are present under native conditions because of incomplete cross-linking. In all cases, the protein concentration was 1 μM, and the buffer was as reported in the legend for Figure 2.

thoroughly denatured protein (Figure 5C). The majority of the $-CH_2-$ and $-CH_3$ protons are observed to resonate in sharp peaks near 0.9 ppm, and all of the upfield signals (0.1 to −1.5 ppm) have disappeared. The lone remaining signal at 0.00 ppm is due to the chemical shift standard. The aromatic, αH, and βH regions of the spectrum are also characteristic of an unfolded protein. The amide signals have also collapsed into a narrow zone (8.0 to 8.7 ppm), and the indole protons resonances are also clustered together at 10.0 to 10.2 ppm (Figure 5C, inset). The amide and indole signals indicate that the hydrogen-bonding network of the protein's secondary structure has broken down after 30 min in 8 M urea and that the Trp side chains are unfolded and solvent-exposed. A preliminary spectrum recorded after only 10 min in 8 M urea before the instrument was fully shimmed also reveals characteristics of a thoroughly unfolded protein (data not shown). A series of spectra were recorded overnight (one per hour) on the same sample, and the last one is shown in Figure 5D. These spectra are essentially identical to those recorded after 30 min of unfolding.

Apocystalysin. Equilibrium studies of urea-induced unfolding of apocystalysin were also performed. The far-UV CD spectrum of native apocystalysin is identical to that of holocystalysin, thus suggesting a similar secondary structure composition. Although native apocystalysin displays an emission maximum (λ_{max}= 336 nm) of intrinsic fluorescence equal to that of holocystalysin, its tryptophan emission intensity is higher (∼3-fold) compared to that of the holoenzyme, given the absence of energy transfer to the coenzyme. With respect to the native holoenzyme, apocystalysin exhibits a decrease of negative dichroic bands of 288−296 nm and an increase of the positive band at 275 nm (*6*). The unfolding of apocystalysin by urea was first investigated by CD spectroscopy at 222 and 288 nm as well as by tryptophan fluorescence. Treatment with urea of apocystalysin causes a decrease of the CD signal at 222 nm as the concentration of urea was increased and changes both in the emission maximum and in the emission intensity of tryptophan fluorescence. Figure 6A shows the unfolding profiles of apocystalysin monitored by far-UV CD and the

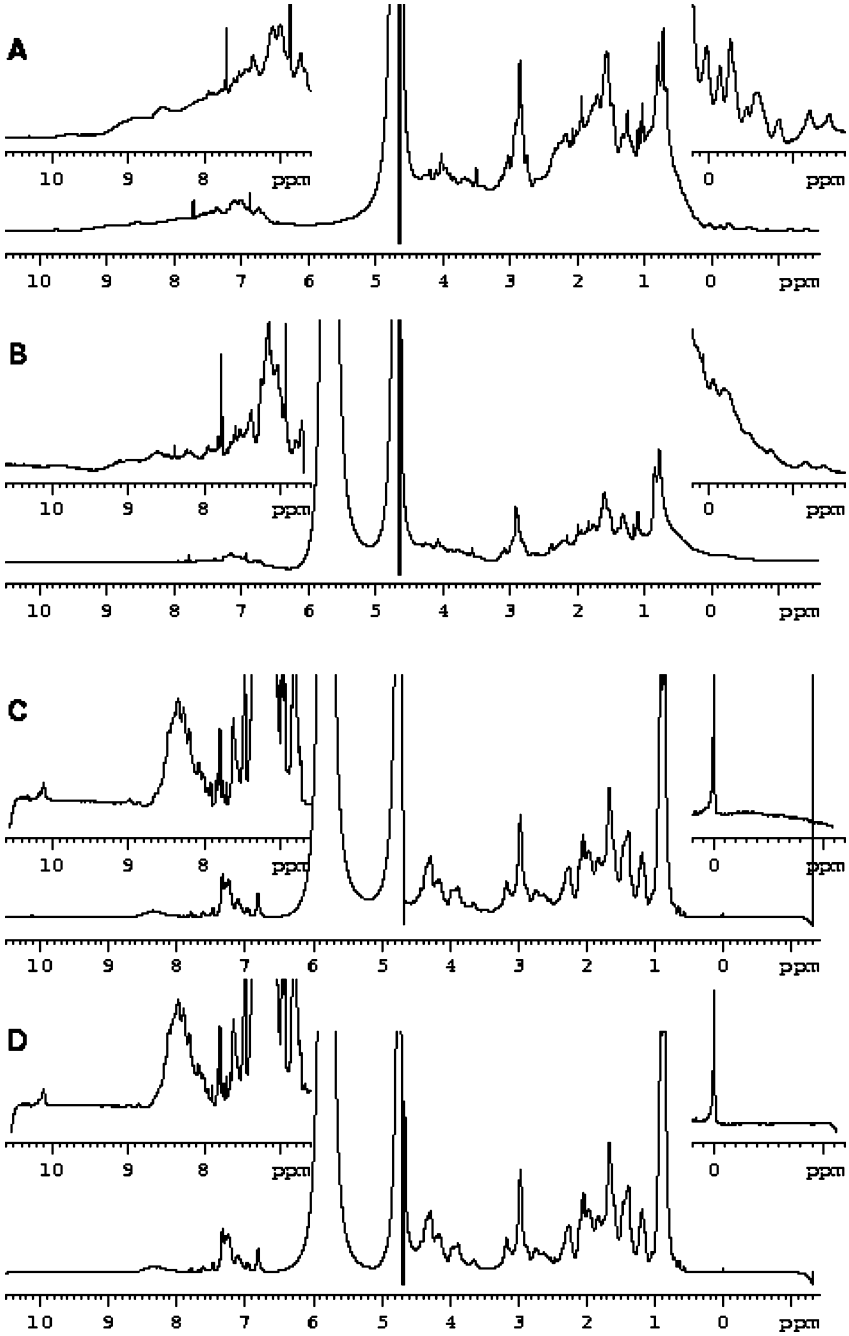

FIGURE 5: Cystalysin unfolding monitored by ^{1}H NMR. All spectra were acquired at 25 °C in 10 mM potassium phosphate buffer, and the pH meter reading was 7.4. The broad signal at 4.7 ppm is due to water, and the very broad signal appearing in panels B, C, and D and centered at 5.8 ppm arises from urea. The sharp peak at 0.00 ppm (inserts in panels C and D) is due to DSS, the internal chemical shift standard. (Panel A) ^{1}H NMR spectrum of holocystalysin without urea, incubated overnight. (Panel B) ^{1}H NMR spectrum of holocystalysin in 4 M urea after overnight incubation. (Panel C) Holocystalysin in 8 M urea. This ^{1}H NMR spectrum was recorded 30 min after the addition of concentrated urea. (Panel D) ^{1}H NMR spectrum of holocystalysin in 8 M urea after overnight incubation.

fluorescence emission maximum. These curves are consistent with a mechanism involving an intermediate state at 2.5−4 M urea. The midpoint of the first and second transitions is reported in Table 1. Different unfolding profiles for holo and apocystalysin are also observed by comparing their intrinsic emission intensity in the presence of increasing concentrations of urea. The overall process of the unfolding of the apoenzyme was found to be triphasic, and an intermediate state, more populated at 1 μM than at 0.1 μM enzyme, appeared to be stable at ~3 M urea (Figure 6B). The transition midpoints measured at 1 μM apoenzyme were at 1.1 ± 0.1, 2.20 ± 0.02, and 4.1 ± 0.1 M urea for the first, second, and third phases, respectively (Table 1). The position of the first transition was dependent on protein concentration (C_{m1} = 0.65 ± 0.08 M urea for 0.1 μM apoenzyme), thus suggesting that this transition is linked to the dissociation of the dimeric apoenzyme. No such dependence was observed for the second and the third transitions, which are coincident with those observed for apocystalysin by fluorescence emission maximum and far-UV CD measurements. At urea concentrations higher than 5 M, the intensity and the maximum emission fluorescence as well as the ellipticity at 222 nm of holo and apoenzymes are very similar. Although the loss of the near-UV CD signal at 288

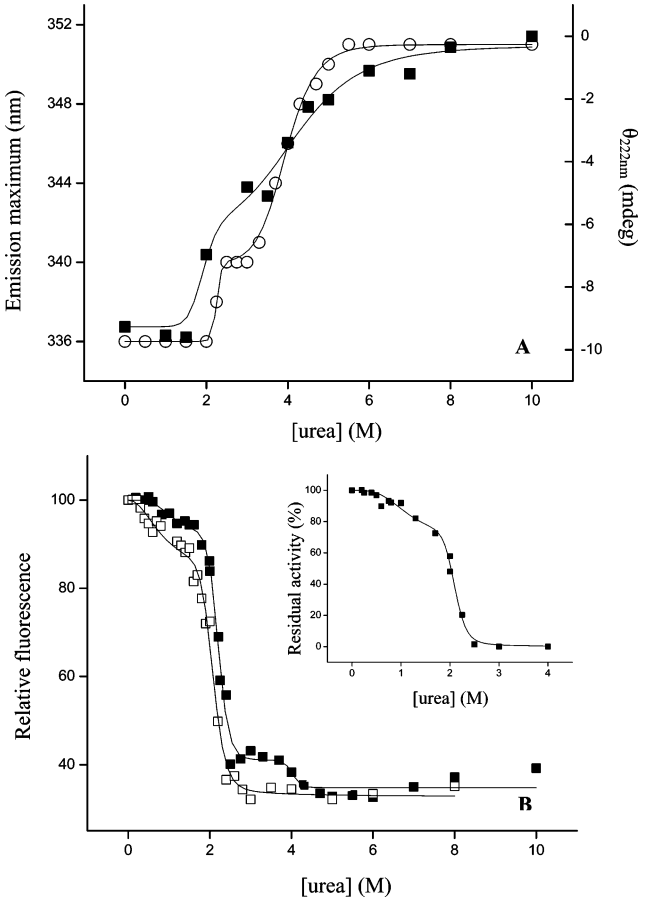

FIGURE 6: Urea-induced unfolding equilibrium of apocystalysin. (A) Unfolding profiles of 1 μM apocystalysin by emission maximum fluorescence (excitation at 281 nm) (○) and far-UV CD at 222 nm (■). (B) Changes in emission intensity protein fluorescence of 0.1 μM (□) and 1 μM (■) apocystalysin. (Inset) Changes in enzymatic activity of apocystalysin (1 μM) (■). The data shown are the means of four independent experiments; the S.E. of the mean (not shown) was less that 5% of the mean value in every case. Solid lines represent the best fit obtained using a three-state denaturation model (eq 2), except for the profile of the emission intensity of 1 μM apoenzyme for which the four-state denaturation model (eq 3) has been used. In all experiments, the buffer was as reported in the legend for Figure 2.

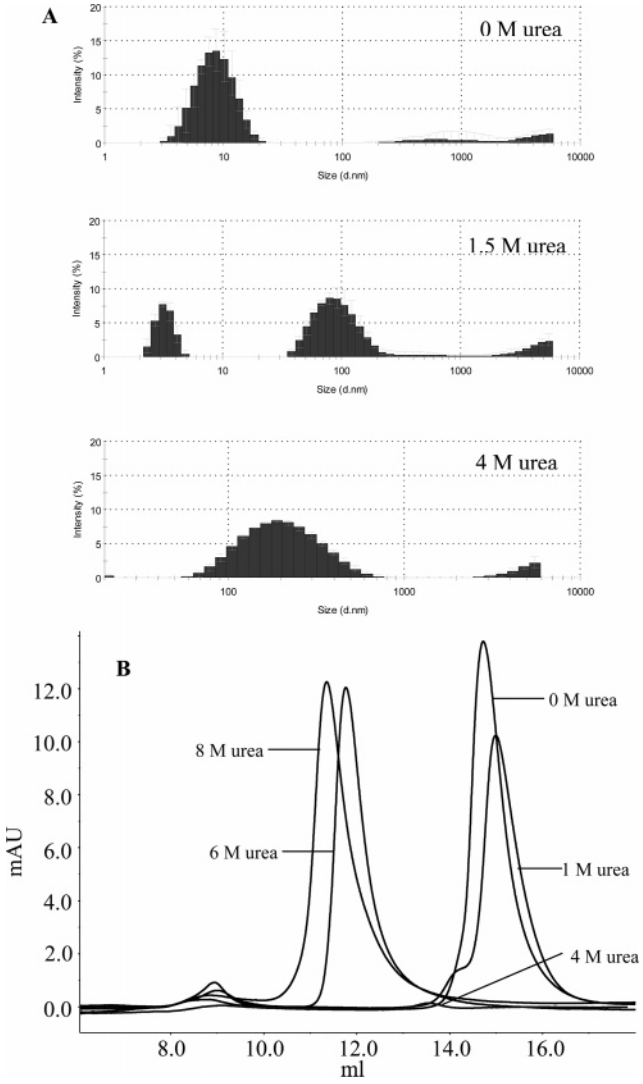

FIGURE 7: Urea-induced changes in molecular dimension of apocystalysin. (A) Size distribution from DLS and (B) chromatographic profiles on the Superdex 200 HR/30 column of apocystalysin at the indicated urea concentrations. In all cases, the protein concentration was 1 μM, and the buffer was as reported in the legend for Figure 2.

nm with the increase of urea concentration could be observed, the achievement of the near-UV unfolding profile is seriously hindered because of the small signal changes and light-scattering effects. Nevertheless, it is worth noticing that the 288 nm signal remains almost invariant in the 0−2 M concentration range of urea, is highly scattered between 2 and 4 M urea, and reaches a value identical to that of holocystalysin under the same experimental conditions at 8 M urea (data not shown). The 1D ^{1}H NMR spectrum of 8 M urea-treated apoenzyme shows the same features of the holoenzyme under the same denaturant condition (data not shown).

Cystalysin in the apo form is more sensitive to an increase in denaturant concentration than cystalysin in the holo form. As reported in the inset of Figure 6B, the overall process describing the loss of catalytic activity was found to be biphasic. A loss of approximately 30% of the enzymatic activity is associated with the first transition ($C_{m1} = 1.1 \pm 0.1$ M urea), whereas the remaining activity was lost through a steep cooperative transition with a midpoint centered at 2.10 ± 0.02 M urea (Table 1). The first transition coincides with the urea-induced unfolding transition observed in emission intensity fluorescence of the apoenzyme, whereas the second transition closely resembles those monitored by the apoprotein fluorescence as well as the first transition observed by far-UV CD.

Altogether, these data indicate the presence of intermediates during the urea-induced unfolding of apocystalysin. The fluorescent phase diagram reported in Figure 3B providing evidence for the existence of at least three independent transitions supports this view.

Like holocystalysin, apocystalysin has a hydrodynamic diameter of 8.5 ± 0.5 nm as detected by DLS (Figure 7A). However, for apocystalysin (1 μM), an increase in the retention volume to 14.6 mL (corresponding to an experimental *R*s of 3.4 nm) compared to 14.3 mL corresponding to native holocystalysin was observed. Unexpectedly, the peak area of the apoenzyme is ~85% with respect to that of the holenzyme at the same concentration. Because the 280 nm absorbance contribution of PLP is less than 2%, it is difficult to explain the reason for peak area discrepancy

between holo and apoenzyme. The effect of increasing urea concentrations on the molecular size of apocystalysin has been investigated. Between 0 and 2 M urea, the dimeric species of apoenzyme is gradually converted to a monomeric species. The monomer is detected by DLS experiments at 1.5 M urea as the species with a hydrodynamic diameter of 3.3 ± 0.2 nm (Figure 7A). Over this urea range, the enzyme eluted as a single peak whose retention volume gradually increases (for the interpretation of this shift, see below). In addition, the integrated total peak area in the chromatogram begins to decrease significantly, reaching a minimum value of about 2% relative to the native protein in the 2.5−4 M urea range (Figure 7B). For the 4 M urea-treated apoenzyme, DLS measurements show a peak corresponding to particles with a size of ∼220 nm (Figure 7A). When the urea concentration is increased further, the fraction of the insoluble aggregates was converted into the soluble unfolded monomeric form, as made evident by the recovery of the total area of the peak eluted with a significantly reduced volume (11.4 mL, a value identical to that of holocystalysin under the same experimental conditions) (Figure 7B). Glutaraldehyde cross-linking experiments of apocystalysin at different urea concentrations show a decrease in the dimer-to-monomer ratio between 0 and 2 M urea, indicating the formation of a monomeric intermediate. Only large aggregates are detected at 4 M urea. At high denaturant concentration (8 M), a single band corresponding to a monomeric species is observed (data not shown).

Upon the addition of native apocystalysin, ANS fluorescence displays an emission wavelength maximum at 485 nm and an ∼6-fold increase of fluorescence emission intensity. These data suggest a significantly higher exposure of hydrophobic patches in native apocystalysin compared with that of holocystalysin. The addition of ANS to apocystalysin treated with increasing concentrations of urea reveals that (i) both the emission maximum and intensity remain unchanged up to 2 M urea, (ii) the precipitation of apoprotein occurs between 2 and 4 M urea, and (iii) the emission maximum gradually increases, reaching the same value as that of the probe alone in 8 M urea.

Changes in the composition of the secondary structure of 1 μM apocystalysin in the presence of 3 M urea, where aggregates are predominant, were monitored kinetically by recording and analyzing a series of far-UV CD spectra. On the basis of CD data, the native apoenzyme exhibits a composition of secondary structure elements similar to that of the holoenzyme. With time, a remarkable loss of α-helical secondary structure and a concomitant enrichment of β structure could be observed. No significant changes in the amount of random coil were seen. The observed changes in both helix and β structure contents show first-order rate constants of approximately 4 h^{-1} (data not shown). This indicates that an α-helix to β-sheet conformational change is associated with apocystalysin aggregation.

Refolding Studies and Associative Behavior of Cystalysin. The refolding efficiency of holo and apocystalysin was studied kinetically by monitoring the time courses of changes in enzymatic activity following a 100-fold dilution of urea-treated proteins. Starting from the fully denatured holoenzyme (1 μM at 8 M urea), the rate of recovery of enzyme activity was considerably slow, taking about 15 h to reach the final value corresponding to ∼40% of the initial activity.

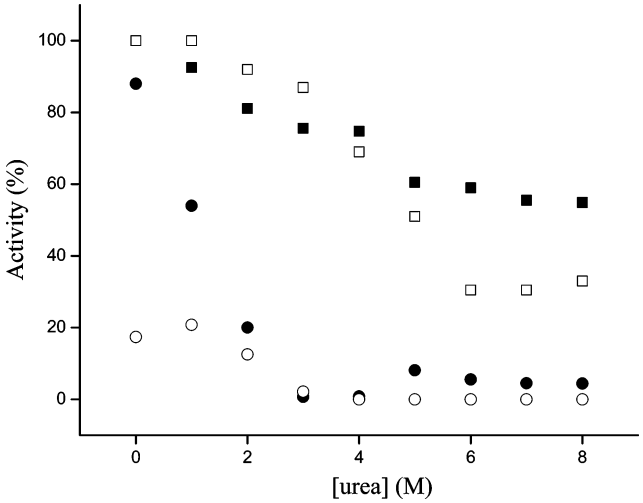

FIGURE 8: Reactivation yield of holo and apocystalysin by dilution. Holocystalysin, 1 μM (□) or 5 μM (■), and apocystalysin, 1 μM (○) or 5 μM (●), were denatured for 15 h in various concentrations of urea as indicated on the *x*-axis. Refolding was induced by 100-fold dilution. The activity data are expressed as the percentage of activity of the corresponding holo and apoenzymes treated in the absence of denaturant under the same experimental conditions. In all experiments, the buffer was as reported in the legend for Figure 2.

The presence of dithiothreitol was mandatory in the refolded mixture to obtain significant refolding; in its absence, just 2% of activity was regained. However, following the unfolding of 1 μM apocystalysin with 8 M urea and its refolding by 100-fold dilution, the enzyme refolded in the presence of dithiothreitol only shows ∼2% of the initial specific activity. When holo or apocystalysin were equilibrated for 15 h at 25 °C with different urea concentrations and then diluted to a final concentration of 10 or 50 nM protein, the yield of reactivation was strongly influenced by the concentration of urea used (Figure 8). At urea concentrations below 4 M, the recovery of catalytic activity for the holoenzyme was 80−100% and not significantly dependent on protein concentration. Instead, partial reversibility, which increases at higher protein concentration, was observed in holoenzyme samples at higher urea concentrations (4−8 M). It is also apparent, however, from Figure 8 that at urea concentrations above 3 M, the efficiency of renaturation for the apoenzyme is very low and independent of protein concentration, whereas below 3 M, the renaturation yield reaches 20 and 60% at 10 and 50 nM protein concentration, respectively. Taken together, these data suggest that at least at the samples conditions used for these experiments, the refolding equilibrium in the concentration range 4−8 M urea (holoenzyme) and 0−3 M urea (apoenzyme) is governed by a reassociation step. Therefore, we decided to investigate the dissociation/association process of cystalysin.

Holocystalysin eluted from gel filtration as a single peak with an elution volume corresponding to a dimer. The elution volume remains unchanged when the concentration was in the range 0.1−30 μM. On the contrary, over the same range, apocystalysin eluted as a single peak, whose position varied between the dimeric and monomeric enzyme. At higher concentrations, the peak position of apocystalysin was closer to that of the dimeric enzyme, whereas at lower concentrations, it was closer to the monomer position. All elution profiles had comparable shapes, representing a mixture of

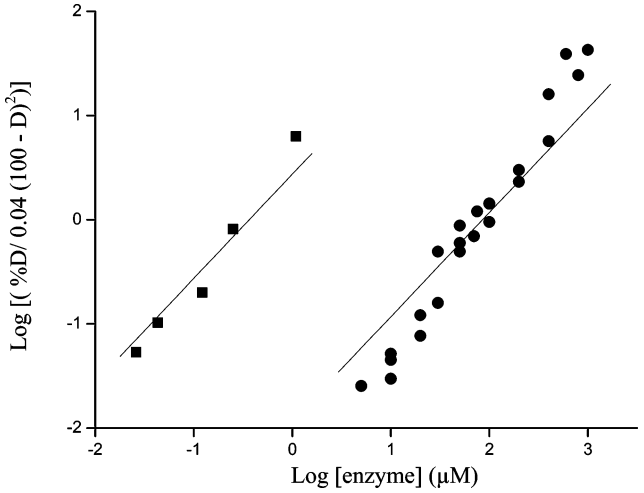

FIGURE 9: Dimer-monomer K_d values of apocystalysin in the absence or presence of PLP. (●), percentage of the dimer to total apocystalysin or (■), maximal specific activity measured upon the additon of 100 μM PLP to apocystalysin as a function of enzyme concentration. The procedures are described in the text. The solid lines represent the best fit obtained using eq 4. In all experiments, the buffer was as reported in the legend for Figure 2.

monomeric and dimeric apocystalysin in rapid equilibrium. The percentage of dimer present can be estimated readily from the elution position of the peak relative to the elution volumes for the monomer and dimer. A plot of the percent apocystalysin dimer as a function of apocystalysin concentration gave a hyperbolic-like curve. Figure 9 shows a linear transformation of these data, whose abscissa intercept yields the dimer−monomer dissociation constant $K_d = 0.37 \pm 0.08$ μM.

As expected, when the lyase activity of cystalysin was measured at saturating β-chloro-L-alanine concentration as a function of enzyme concentration (ranging from 0.01 to 1 μM) a k_{cat} value of $\sim$44 s^{-1} (*3*) was found at all enzyme concentrations tested. The same k_{cat} value is obtained when apocystalysin was diluted to a final concentration ranging from 0.01 to 1 μM in a buffer solution containing 100 μM PLP. On the contrary, if PLP is added to diluted solutions of apocystalysin, the k_{cat} values of apocystalysin measured in the presence of exogenous PLP (100 μM) exhibit a hyperbolic-like curve as a function of protein concentration. The dissociation constant (K_d), determined by a log−log plot of enzyme concentration (as dimer) versus percent k_{cat} (Figure 9), was found to be 0.085 ± 0.03 μM, $\sim$4-fold lower than that determined in the absence of PLP.

Taken together, these data indicate that (1) the association of monomers to form active dimers is a rapid process and that (2) the binding of the coenzyme decreases the equilibrium dissociation constant of the enzyme. Moreover, this K_d value serves as the basis to understand why the reactivation of cystalysin is more efficient at 50 nM compared to that at 10 nM; namely, the formation of the dimer is favored at the higher concentration. This effect is, of course, more pronounced for apo than for holocystalysin.

To minimize effects due to dimer dissociation, the refolding of 1 μM inactivated holo and apocystalysin was performed by extensive dialysis to remove urea. As shown in Figure 10, the recovery of activity of holocystalysin by dialysis is slightly higher than that previously observed for the holoenzyme refolded by dilution to a final protein concentration of 50 nM and roughly corresponds to the percentage of dimeric species found in the refolded species. Moreover, the total peak area in the chromatograms decreases for holocystalysin refolded after denaturation at urea concentrations of 3 and 4 M urea to about 80% of that measured for the untreated holoenzyme. These results clearly indicate the presence of insoluble aggregates in these refolded solutions.

When the refolding reaction was performed in the absence of the coenzyme (apocystalysin), we found a lower recovery of the soluble protein in the 2−8 M urea range than that observed for the refolded holoenzyme. The lowest recovery occurs at 3 M urea. Size-exclusion chromatography indicates that the soluble refolded species consists of two peaks whose retention volumes correspond to the dimer and monomer, with the monomer being more abundant at 2 M urea than at higher urea concentrations. Considering that the above-reported experiments have indicated a rapid monomer ↔ dimer equilibrium under native conditions, the presence of two peaks in the refolded solutions is diagnostic of a slow monomer−dimer interconversion. Because the coenzyme is required for the enzyme to show activity, the regain of activity by apocystalysin was compared with that of the refolded species of apoenzyme upon addition of PLP. It is apparent from Figure 10 that after incubation of the refolded solutions with PLP (100 μM), the peak corresponding to the monomer when it is present is converted to a dimeric species. The integrated areas for the dimer, expressed as the percentage of the area of the untreated enzyme, are within the limits of the experimental errors consistent with the percentage of the enzymatic activity of the sample.

The significance of *in vitro* refolding experiments depends to some extent on establishing that the properties of the refolded protein are equivalent to those of the original native enzyme. To compare renatured holocystalysin with its native enzyme, the renatured dimer was collected. The profiles of the native and renatured enzymes in a Sephadex 200 gel filtration chromatography column were identical. Furthermore, there are no significant differences between the fluorescence and CD properties of the native and reassociated dimers (data not shown). This implies the restoration of the native environment around the aromatic residues and the full acquisition of the native secondary structure.

DISCUSSION

Folding Pathways of Cystalysin in the Holo and Apo Forms. The simplest mechanism that accounts for all experimental observations on urea-unfolding of *T. denticola* cystalysin in the holo form is depicted in Scheme 1. The urea-induced unfolding of holocystalysin is a multistep process yielding detectable intermediates, whose formation is evidenced by the following points: (i) unfolding curves monitored by far--UV CD, near-UV CD, and fluorescence do not coincide with the curves detected by activity and visible CD, (ii) upper field NMR signals are broadened at 4 M urea, even if this effect could be also due to the higher viscosity of 4 M urea relative to buffer without urea, (iii) protein tends to aggregate at 4 M urea, and (iv) the hydrodynamics dimension gradually increases up to 5 M. This issue is also addressed by the phase diagram, revealing

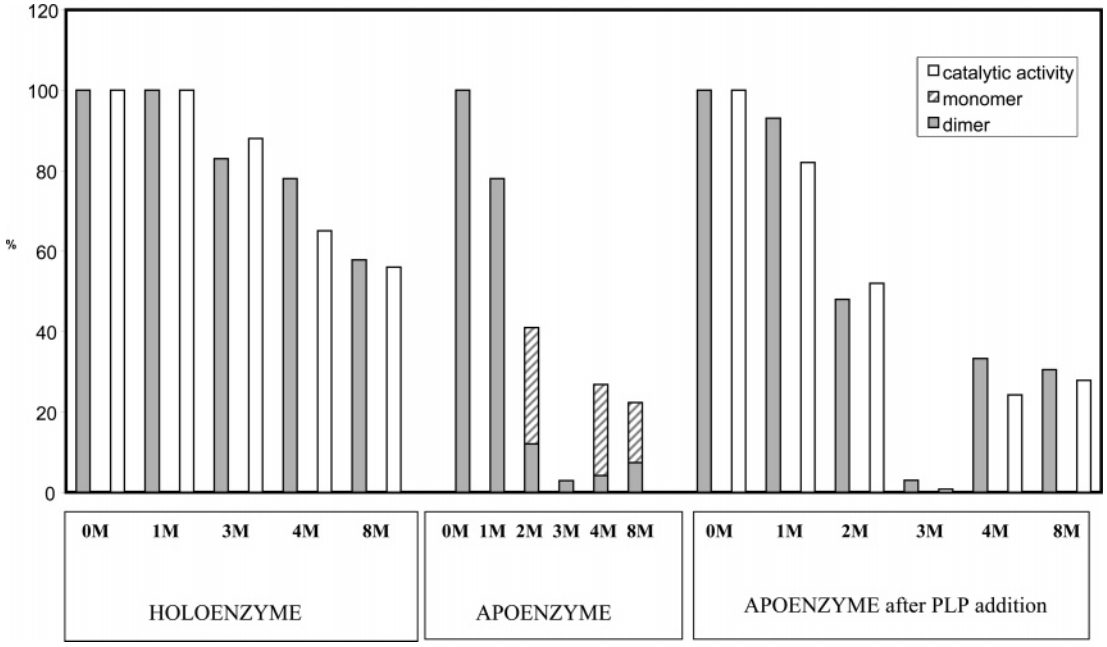

FIGURE 10: Refolding yield of holo and apocystalysin by dialysis. Holo and apocystalysin (1 μM) were denatured for 15 h at the indicated urea concentrations and then subjected to an extensive dialysis against 20 mM potassium phosphate buffer at pH 7.4, containing 0.5 mM dithiothreitol, in the presence or absence of PLP, respectively. Samples are assayed either for their enzymatic activity or for their oligomerization state by gel filtration on a size-exclusion column. The histograms represent the percentage of enzymatic activity or soluble protein with respect to those of holo and apoenzymes treated under the same experimental conditions but in the absence of denaturant. Data shown are means of three independent experiments; the standard deviation from the mean was less than 10% in all cases.

Scheme 1: Folding Pathway of Holo and Apocystalysin[a]

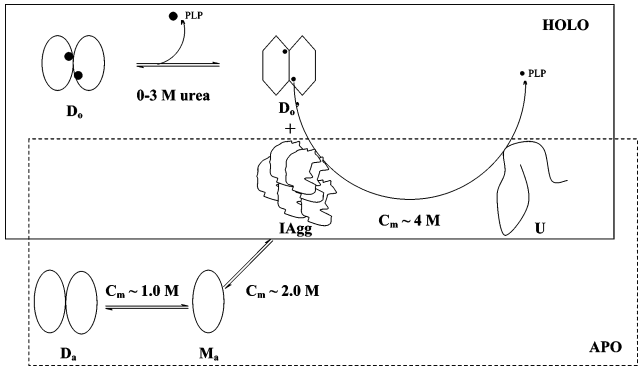

[a] D_o and D'_o indicate the dimeric native and the extended conformation of holocystalysin, respectively; D_a and M_a indicate the dimeric native apoenzymes and the apomonomer, respectively; and IAgg represents the insoluble oligomers and U the unfolded monomer.

the presence of two intermediates. The first step, occurring over the 0−6 M urea range, is associated with the release of PLP, complete inactivation, and the loss of a large portion of the tertiary and secondary structures. The progressive loss of coenzyme causes an equilibrium mixture of essentially the dimer and higher oligomers. The dimer adopts a partially unfolded and greatly expanded conformation, possibly due to the loosening of the interface interactions. Cross-linking experiments indicate that aggregation occurs via a transient apomonomer intermediate. The formation of aggregates is in general consequent to the exposure of sticky surface hydrophobic sites/patches. However, the unfolding of holocystalysin causes no detectable change in the fluorescence emission intensity of ANS over the entire range of denaturant tested, ruling out that additional hydrophobic clusters become superficial as the urea concentration increases. Considering that the surface of cystalysin is endowed with a high positive charge electrostatic character (*5*), it can be suggested that the small fraction of ANS binding may be due to the ability of ANS to bind to cationic groups of the protein (*26*). The subsequent event is the concomitant dissociation of aggregates and complete denaturation producing an extended fully unfolded monomeric species. The absence of protein concentration dependence in this step arises from the very high degree of structural destabilization required to produce monomerization so that no intermediate states having spectroscopic properties significantly different from those of the native dimer or the unfolded monomer are populated at equilibrium.

For apocystalysin, a pathway of urea-induced unfolding involving intermediates detected on the basis of unfolding profiles, and a phase diagram could be proposed (Scheme 1). The emission fluorescence intensity of apocystalysin displays a first transition with a midpoint of ~1.1 M urea, which is protein concentration dependent. This transition, coincident with that involving a partial loss of enzymatic activity, is not accompanied either by a shift in the emission maximum fluorescence or by a change in the far-UV CD signal and entails monomerization. Thus, unlike for holocystalysin, the dissociation of folded fully active dimer of apocystalysin occurs at low urea concentration. The monomeric species retains almost all of the native secondary and tertiary structures but is characterized by a small conformational change, possibly confined to the active site. Following monomerization, a transition takes place leading to an equilibrium unfolding intermediate stabilized at ~3 M urea, which retains ~45% of the native CD signal and ~40% of the native fluorescence. The structure of this intermediate consists of insoluble aggregates of high molecular weight, which, on the basis of kinetic unfolding CD data, are characterized by a higher content of β structure with respect to the native enzyme. Thus, intermolecular contacts giving

Table 2: Comparison between Monomer Interfaces of Cystalysin and MalY

	cystalysin	MalY
interface accessible surface area (Å^2)	1905.61	1753.96
% interface accessible surface area	11.23	11.68
% polar atoms in interface	31.23	30.55
% non-polar atoms in interface	68.77	69.40
hydrogen bonds	16	16
salt bridges	0	0
disulphide bonds	0	0
gap volume (Å^3)	10835.91	7674.94
bridging water molecules	0	8

rise to aggregates could involve β-sheet-like interactions. Interestingly, an increase in β-sheet structure accompanies the formation of amyloid, a conformational state implicated in over 20 fatal human diseases (*27*, *28*). Hydrophobic interactions could be responsible for the propensity of the partially unfolded monomer to self-associate. This is also expected, considering the computed highly hydrophobic nature of the subunit interface (Table 2). In fact, the value of accessible surface areas (*ASA*s), which become exposed upon dissociation, corresponds to ~11% of the total protein surface area, and the large fraction (~69%) of the surface becoming accessible is represented by hydrophobic residues. However, the addition of ANS to apocystalysin does not lead to any ANS-bound intermediate over the entire urea range but causes an immediate precipitation of the protein between 2 and 4 M urea. The inability of the monomeric intermediate to bind ANS may be explained by an occlusion of the ANS binding sites because of intermolecular contacts within the aggregating material. Binding of ANS to the positive charges on the surfaces of aggregates could decrease the electrostatic repulsion between oligomers, leading to further aggregation and protein precipitation (*26*).

A typical strategy to induce refolding of proteins in good yield and avoid aggregation phenomena consists of a quick dilution of the unfolded protein. However, when this method was applied to cystalysin, we observed that the dilution of inactivated holo or apoenzyme to a final protein concentration lower than 85 and 370 nM, respectively, leads to a dramatic drop of reactivation recovery. This could be related to the values of the equilibrium dimer−monomer dissociation constants measured in the presence or absence of PLP. On the basis of these observations and provided that refolding conditions *in vitro* reflect physiological folding conditions, it is reasonable to expect that in *T. denticola*, the concentration of cystalysin would be in the micromolar range. Chu and Holt (*1*) reported a concentration of holocystalysin of 0.3 μM in the oral pathogen, and our results suggest that at this concentration, the enzyme is predominantly dimeric. Nevertheless, we also realize that at the optimal protein concentration (1 μM), where the rate-limiting step in the refolding does not depend maximally on the pairing of subunits to give dimeric conformation, a partial regain of activity from fully denatured protein (50−60% in the presence of PLP and 20−30% in its absence) was obtained. When the unfolding of urea-treated cystalysin was followed by extensive dialysis, the reactivation yield of both holo and apocystalysin was lower and higher when the protein was denatured in high ($\geq$3 M) or low ($<$3 M) concentrations of urea, respectively. Almost no reactivation could be observed for the apoenzyme denatured at 3 M urea, where nearly all of the enzyme is in the aggregate form. Efficient reactivation of the unfolded enzyme can be achieved only before aggregation. These data, together with the formation of insoluble aggregates during refolding, indicate that under these experimental conditions, enzyme reactivation is mostly limited by an aggregation step. Moreover, the finding that PLP enhances the yield of properly active enzyme suggests that the binding of the coenzyme favors proper folding and association by inhibiting the aggregation of the refolded enzyme with the incompletely or incorrectly folded protein. The possibility that PLP could bind to a monomeric intermediate during the refolding process could be taken into consideration. Although a rapid monomer $\leftrightarrow$ dimer equilibrium was observed for apocystalysin under native conditions, a slow monomer−dimer interconversion was noted during refolding. It is possible that a monomeric species arising during refolding and possessing a distorted conformation of the PLP pocket can slowly assemble to a dimer. The slow cis $\leftrightarrow$ trans isomerization of proline peptide bonds has been found to greatly slow the refolding of many proteins (*29*). In this regard, it is of interest that three *cis*-proline peptide bonds (Thr120−Pro121, Ser172−Pro173, and Asn175−Pro176) are close to each other and to the PLP-binding site. Notably, Herold and Leistler (*30*) have proposed that PLP binds to a monomeric folding intermediate in aspartate aminotransferase from *E. coli*. However, considering that the coenzyme-binding cleft of native cystalysin is composed of residues belonging to adjacent subunits, it cannot be ruled out that a dimerization step precedes the genesis of PLP-binding capability. Several *in vitro* refolding studies have shown that for other PLP-dependent enzymes, such as the β_2 subunit of tryptophan synthase (*31*) and the cytosolic aspartate aminotransferase (*32*), the coenzyme favors the reactivation. It should be pointed out that the association of monomers and the stabilization of the native dimer by coenzyme binding may constitute an additional pathway to the folded dimer, thereby minimizing misfolding and misassembly.

How Do the Dimerization and the Equilibrium Folding Processes of Cystalysin and MalY Compare? The associative behavior and the folding pathway of cystalysin can be compared to those of MalY, another PLP-binding enzyme whose denaturation has been recently investigated (*9*). Cystalysin from *T. denticola* and MalY from *E. coli* are members of the α family and fold type I of PLP enzymes and are characterized by a similar active site architecture. Their sequences are 27% identical and 48% similar, being the major variations dispersed through their sequence. Both these enzymes are catalytically active as dimers and belong to the group of Cβ-Sγ lyases that produce ammonium and pyruvate. On the basis of their crystal structures (*5*, *33*) and their catalytic properties, a common catalytic mechanism has been proposed (*5*, *33*). Notwithstanding these similarities, the two enzymes exhibit a difference in their association/dissociation process. Unlike cystalysin, the monomer−dimer equilibrium has been found to be slow for MalY (*9*). In addition, from previous data (*9*), it can be deduced that equilibrium dissociation constants for Mal Y are $<$0.1 μM and $\ll$0.1 μM in the absence or presence of PLP, respectively. It may be physiologically relevant that MalY persists in a dimeric structure at low protein concentrations because it is biologically active as a dimer, either in exhibiting

cystathionase activity or in repressing the maltose system by forming a complex with MalT (*34*). The comparative analysis carried out on the subunit interface shows no significant differences between cystalysin and MalY, except for the number of bridging water molecules and the gap volume (Table 2). Considering that the gap volume gives a measure of the complementarity of the interacting surfaces (*35*), the higher value of the equilibrium dimer−monomer dissociation constants of cystalysin compared to those of MalY could be ascribed to a lower complementariness of the interacting surfaces for cystalysin compared to that for MalY.

Both enzymes in the apo form seem to follow the same unfolding pathway, including monomerization, the formation of aggregates, and complete unfolding of monomers. The existence of a self-associated intermediate in the folding pathway of apocystalysin is similar to what occurs in MalY, although structures of the self-associated intermediates might not necessarily be identical in every detail. Although both these intermediates, even to a different degree, are characterized by a higher content of β structure with respect to the corresponding native enzymes, the rate constant of their formation is higher for cystalysin than for MalY. Again, the aggregates formed during the folding of apocystalysin are insoluble, whereas those of apoMalY are soluble. However, the comparison of unfolding pathways of holocystalysin and holoMalY reveals that (i) the visible CD-detected C_m is ~1.5 M (*9*) and ~3 M urea for holoMalY and holocystalysin, respectively, (ii) the unfolding pathways of holo and apoenzyme were very similar at urea concentrations higher than 2 and 5 M for MalY and cystalysin, respectively, and (iii) holoMalY loses a large portion of secondary and tertiary structures at concentrations of denaturant higher than the concentration at which dimer dissociation occurs, whereas holocystalysin undergoes a concerted process involving the monomerization and disruption of secondary and tertiary structures. This implies that PLP bound to cystalysin is maximally responsible for the intermonomer interactions and that a high degree of unfolding is required for monomerization. It can be suggested that the structural PLP domains could be differently stabilized by interaction with PLP in holoMalY and holocystalysin. In both cystalysin and MalY, the PLP cofactor is located in a wide catalytic cleft that is assembled by residues from both subunits of each enzyme. Although holocystalysin displays a dense network of interactions between the coenzyme and protein matrix, MalY binds the PLP phosphate through five water molecules and entails only one interaction with a protein residue (Tyr 61*). This could imply that the PLP domain, or at least a portion essential for intersubunit interactions, is more resistant to unfolding in holocystalysin than in holoMalY. Consequently, the dissociation of holocystalysin begins at a higher denaturant concentration in comparison with that of holoMalY.

Another striking difference between MalY and cystalysin concerns their refolding mechanism. The refolding of MalY proceeds either in the presence or absence of PLP, whereas cystalysin requires PLP for reactivation. Undoubtedly, PLP's role in both proteins is to stabilize the dimeric structure essential for their biological activities. This effect appears to be more important in cystalysin than in MalY. On the basis of a number of interactions of PLP with the protein matrix higher in cystalysin than in MalY, it is reasonable to suggest that PLP could bind to some early semi-structured (monomeric) intermediate of cystalysin, thus possibly reducing the conformational freedom of the polypeptide. This event could be less likely for MalY because the coenzyme appears to be unable to interact with non-native protein states and only becomes incorporated during the final steps of protein folding.

CONCLUSION

The results of the comparative studies on the association equilibrium monomer ↔ dimer and on the folding pathway for holo and apocystalysin indicate the effect of PLP in these processes. Binding of the coenzyme stabilizes the native conformation in its dimeric structure. Urea-induced unfolding profiles show that monomerization of apocystalysin occurs at low denaturant concentration without the significant loss of secondary and tertiary structures, whereas it takes place for holocystalysin at high denaturant concentration, once the structure is sufficiently destabilized.

In addition, the dimerization and folding processes of *T. denticola* cystalysin have been compared with those of *E. coli* MalY, a Cβ-Sγ PLP lyase, which shares with the former enzyme a significant structural resemblance and a common catalytic mechanism. Evidence is provided for different dynamics of their subunit dissociation/association processes, possibly related to the different extent of the complementarity of their interacting surfaces. The importance of the relationship between the role of coenzyme binding during protein folding and the topology of its binding site in native protein has been also highlighted.

ACKNOWLEDGMENT

We thank Professor F. Chiti (University of Firenze, Italia) for the use of the DLS facility.

REFERENCES

1. Chu, L., and Holt, S. C. (1994) Purification and characterization of a 45 kDa hemolysin from *Treponema denticola* ATCC 35404, *Microb. Pathog. 16*, 197−212.
2. Chu, L., Burgun, A., Kolodrubertz, D., and Holt, S. C. (1995) The 46-kilodalton-hemolysin gene from *Treponema denticola* encodes a novel hemolysin homologous to aminotransferases, *Infect. Immun. 63*, 4448−4455.
3. Bertoldi, M., Cellini, B., Clausen, T., and Borri Voltattorni, C. (2002) Spectroscopic and kinetic analyses reveal the pyridoxal 5′-phosphate binding mode and catalytic features of *Treponema denticola* cystalysin, *Biochemistry 41*, 9153−9164.
4. Bertoldi, M., Cellini, B., Paiardini, A., Di Salvo, M., and Borri Voltattorni, C. (2003) Treponema denticola cystalysin exhibits significant alanine racemase activity accompanied by transamination: mechanistic implications, *Biochem. J. 371*, 473−483.
5. Krupka, H. L., Huber, R., Holt, S. C., and Clausen, T. (2000) Crystal structure of cystalysin from *Treponema denticola:* a pyridoxal 5′-phosphate-dependent protein acting as a haemolytic enzyme, *EMBO J. 19*, 3168−3178.
6. Bertoldi, M., Cellini, B., D' Aguanno, S., and Borri Voltattorni, C. (2003) Lysine 238 is an essential residue for α,β-elimination catalyzed by *Treponema denticola* cystalysin, *J. Biol. Chem. 278*, 37336−37343.
7. Cellini, B., Bertoldi, M., Paiardini, A., D'Aguanno, S., and Borri Voltattorni, C. (2004) Site-directed mutagenesis provides insight into racemization and transamination of alanine catalyzed by *Treponema denticola* cystalysin, *J. Biol. Chem. 279*, 36898−36905.
8. Cellini, B., Bertoldi, M., Montioli, R., and Borri Voltattorni, C. (2005) Probing the role of Tyr 64 of *Treponema denticola*

cystalysin by site-directed mutagenesis and kinetic studies, *Biochemistry 44*, 13970−13980.
9. Bertoldi, M., Cellini, B., Laurents, D. V., and Borri Voltattorni, C. (2005) Folding pathway of the pyridoxal 5′-phosphate C-S lyase MalY from *Escherichia coli*, *Biochem. J. 389*, 885−898.
10. Peterson, E. A., and Sober, H. A. (1954) Preparation of crystalline phosphorylated derivatives of vitamin B6, *J. Am. Chem. Soc. 76*, 169−175.
11. Pace, C.N., Shirley, B.A., and Thomson, J. T. (1989) Measuring the conformational stability of a protein, in *Protein Structure, a Practical Approach* (Creighton, T. E., Ed.) pp 311−330, IRL Press, Oxford, England.
12. Neidle, A., and Dunlop, D. S. (2002) Allosteric regulation of mouse brain serine racemase, *Neurochem. Res. 27*, 1719−1724.
13. Cellini, B., Bertoldi, M., and Borri Voltattorni, C. (2003) Treponema denticola cystalysin catalyzes β-desulfination of L-cysteine sulfinic acid and β-decarboxylation of L-aspartate and oxalacetate, *FEBS Lett. 554*, 306−310.
14. Böhm, G., Muhr, R., and Jaenicke, R. (1992) Quantitative analysis of protein far UV circular dichroism spectra by neural networks, *Protein Eng. 5*, 191−195.
15. Uversky, V. N. (1993) Use of fast protein size-exclusion liquid chromatography to study the unfolding of proteins which denature through the molten globule, *Biochemistry 32*, 13288−13298.
16. Manning, L. R., Dumoulin, A., Jenkins, J. R., Winslow, R., and Manning, J. M. (1999) Determining subunit dissociation constants in natural and recombinant proteins, *Methods Enzymol. 306*, 113−129.
17. Hubbard, S. J., and Thornton, J. M. (1993) *NACCESS*, Computer Program, Department of Biochemistry and Molecular Biology, University College, London.
18. Lee, B. K., and Richards, F. M. (1971) The interpretation of protein structures: estimation of static accessibility, *J. Mol. Biol. 55*, 379−400.
19. Jung, H. I., Cooper, A., and Perham, R. N. (2002) Identification of key amino acid residues in the assembly of enzymes into the pyruvate dehydrogenase complex of *Bacillus stearothermophilus*: a kinetic and thermodynamic analysis, *Biochemistry 41*, 10446−10453.
20. McDonald, I. K., and Thornton, J. M. (1994) Satisfying hydrogen-bonding potential in proteins, *J. Mol. Biol. 238*, 777−793.
21. Barlow, D. J., and Thornton, J. M. (1983) Ion pairs in proteins, *J. Mol. Biol. 168*, 867−885.
22. Laskowski, R. A. (1995) SURFNET: A program for visualizing molecular surfaces, cavities and intermolecular interactions, *J. Mol. Graphics 13*, 323−330.
23. Kuznetsova, I. M., Turoverov, K. K., and Uversky, V. N. (2004) Use of the phase diagram method to analyze the protein unfolding-refolding reactions: fishing out the invisible intermediates, *J. Proteome Res. 3*, 485−494.
24. Wilkins, D. K., Grimshaw, S. B., Receveur, V., Dobson, C. M., Jones, J. A., and Smith, L. J. (1999) Hydrodynamic radii of native and denatured proteins measured by pulse field gradient NMR techniques, *Biochemistry 38*, 16434−16431.
25. Wüthrich, K. (1986) *NMR of Proteins and Nucleic Acids*, Wiley, New York.
26. Roy, S., Katayama, D., Dong, A., Kerwin, B. A., Randolph, T. W., and Carpenter, J. F. (2006) Temperature dependence of benzyl alcohol-and 8-anilinonaphtalene-1-sulfonate induced aggregation of recombinant human interleukin-1 receptor antagonist, *Biochemistry 45*, 3898−3911.
27. Chiti, F., and Dobson, C. M. (2006) Protein misfolding, functional amyloid and human disease, *Annu. Rev. Biochem. 75*, 333−366.
28. Bennet, M. J., Sawaya, M. R., and Heisenberg, D. (2006) Deposition diseases and 3-D domain swapping, *Structure 14*, 811−824.
29. Schmid, F. X. (1992) The kinetics of unfolding and refolding of single-domain proteins, in *Protein Folding* (Chreighton, T. E., Ed.), pp 197−241, Freeman, New York.
30. Herold, M., and Leistler, B. (1992) Coenzyme binding of a folding intermediate of aspartate aminotransferase detected by HPLC fluorescence measurements, *FEBS Lett. 308*, 26−29.
31. Groha, C., Bartholmes, P., and Jaenicke, R. (1978) Refolding and reactivation of *Escherichia coli* tryptophan synthase beta2 subunit after inactivation and dissociation in guanidine hydrochloride at acidic pH, *Eur. J. Biochem. 92*, 437−441.
32. West, S. M., and Price, N. C. (1989) The unfolding and refolding of cytosolic aspartate aminotransferase from pig heart, *Biochem. J. 261*, 189−196.
33. Clausen, T., Schlegel, A., Schneider, E., Steegborn, C., Chang, Y.-S., Haase, A., Bourenkov, G. P., Bartunik, H. D., and Boos, W. (2000) X-ray structure of MalY from *Escherichia coli*: a pyridoxal 5′-phosphate-dependent enzyme acting as a modulator in *mal* gene expression, *EMBO J. 19*, 831−842.
34. Schreiber, V., Steegborn, C., Clausen, T., Boos, W., and Richet, E. (2000) A new mechanism for the control of a prokaryotic transcriptional regulator: antagonistic binding of positive and negative effectors, *Mol. Microbiol. 35*, 765−776.
35. Jones, S., and Thornton, J. M. (1995) Protein-protein interactions: a review of protein dimer structures, *Prog. Biophys. Mol. Biol. 63*, 31−165.

BI061496L